

Research papers

State of health estimation of lithium-ion batteries based on Mixers-bidirectional temporal convolutional neural network

Jingyi Gao^a, Dongfang Yang^{b,*}, Shi Wang^c, Zhaoting Li^d, Licheng Wang^e, Kai Wang^{a,f,**}^a School of Electrical Engineering, Weihai Innovation Research Institute, Qingdao University, Qingdao 266000, China^b Haqiang College of Shaanxi University of Science & Technology, Xi'an 712046, China^c Key Laboratory of Intelligent Information Processing, Institute of Computing Technology, Chinese Academy of Sciences, Beijing, China^d School of Engineering, Brown University, Providence, RI 02912, USA^e School of Information Engineering, Zhejiang University of Technology, 310014, Hangzhou province, China^f Shandong Suoxiang Intelligent Technology Co., Ltd, Weifang 261101, China

ARTICLE INFO

Keywords:

Lithium-ion battery
State of health estimation
Bidirectional temporal convolutional neural network
Mixers
Transfer learning

ABSTRACT

Accurate state of health (SOH) estimation is essential for designing a safe and reliable battery management systems (BMS). Although data-driven methods have achieved great accuracy and satisfied robustness in SOH estimation, for most neural networks, it is a challenge for SOH estimation to learn long dependencies in the training process due to the lack of the scalability for modeling long sequences. In this study, a novel SOH estimation framework combing Mixers and bidirectional temporal convolutional neural network (BTCN) is proposed, which not only takes the greatest advantage of local and global properties of input features to estimate SOH of lithium-ion batteries (LIBs), but also eases the redundancy of temporal and channel information. In the data pre-processing, the voltage change in the equal time interval is extracted from the measured data of the constant current (CC) charging stage, which is easily obtained in the real-world charging scenario. Then, the features that are highly correlated with SOH are selected by Pearson correlation coefficient (PCC), and all the features are normalized by minimum-maximum scaling method to speed up the convergence process and reduce the initialization requirement of learning-rate. After pre-processing, all features are input into the Mixers-BTCN model. We carry out experiments on aging data from two public datasets, NASA and CALCE. The simulations results indicate that the R^2 for each dataset is above 0.768. The mean absolute error (MAE) and root mean square error (RMSE) that are both held within 2.34 %, which proves the accuracy and stability of the proposed SOH estimation. In addition, the introduction of transfer learning technology verifies the robustness of the proposed model to different ambient temperatures.

1. Introduction

In the process of automobile electrification, the core is the development of battery technology. Lithium-ion batteries have the merit of high energy density and high cycle efficiency, which is suitable for the energy storage system of electric vehicles (EV) [1–3]. The battery management system (BMS) has been widely used in various powered scenarios, since it can monitor the battery performance, prolong the service life and improve the usage safety. Precise SOH estimation can effectively prevent battery thermal runaway and other operational failures, which is the core competency of a BMS [4–6]. The SOH is generally defined as the ratio of current capacity to initial capacity, as

shown in (1):

$$\text{SOH} = \frac{C_{\text{cur}}}{C_{\text{new}}} \times 100\% \quad (1)$$

However, the lithium-ion battery is a dynamic and time-varying electrochemical system with complicated internal mechanisms [7–10]. With the long-term operation of lithium-ion batteries, both physical mechanisms and chemical mechanisms lead to performance degradation, manifested as SOH decline and power attenuation [11]. It is worth noting that these degradation mechanisms are highly related to the material characteristics of the battery itself, and most of them cannot be studied independently [12–14]. Currently, there is an increasing volume

* Corresponding author.

** Correspondence to: School of Electrical Engineering, Weihai Innovation Research Institute, Qingdao University, Qingdao 266000, China.

E-mail addresses: dongyang_dongyang@126.com (D. Yang), wkwj888@163.com (K. Wang).

of literature on SOH estimation, leading to a plenty of methods. Broadly, these methods can be classified into model-based approaches and data-driven strategies for practical engineering applications. [15–17].

The models for SOH estimation contain electrochemical models (EMs) [18] and equivalent circuit models (ECMs) [19–21], both of which attempt to construct mathematical or physical models describing the decay behavior of batteries. Drawing from the electrochemical theory of lithium-ion batteries, the Electrochemical Models (EMs) establish a nonlinear relationship between the measurement signal and the State of Health (SOH). [22]. This approach inevitably has low robustness and generalization ability because of the variability of lithium-ion battery types and operating conditions. In the ECM model, basic resistors or capacitors components are used to reproduce the electrical behavior of the battery and the parameters are updated by using various filtering algorithms such as Kalman filter (KF) and least square filter [23]. Significant research focus has been directed towards the Kalman Filter (KF). Enhanced versions of KF, like the Extended Kalman Filter (EKF) [24], Unscented Kalman Filter (UKF) [25], and Adaptive Extended Kalman Filter (AEKF) [26], have been developed for strongly nonlinear models, thereby augmenting the robustness and precision of the conventional KF. In general, the accuracy of SOH estimation results is highly associated to the established battery model, and the calculation cost increases with the improvement of the accuracy of the model. Such so, the accuracy of this algorithm in online state estimation is limited by its computational costs and the dynamic adaptability [27,28].

The data-driven methodology leverages battery data comprehensively to extract degradation insights. It then constructs a mapping relationship between health indicators (HIs) and the State of Health (SOH) using artificial intelligence techniques, notably machine learning (ML) [29–32]. They do not need to consider the chemical mechanism of the battery, but need external measurement data as support. A novel SOH estimation method is proposed by Li et al. [33] based on Antlion optimization algorithm and support vector regression (ALO-SVR). [34] combines both ICA-based features and the backpropagation (BP) neural network to establish a multistage SOH estimation model with a broad scope of applications. A novel approach of health indicators (HIs) extraction based on the U-chord curvature model is proposed in [35], and evaluates the estimation performance of gaussian process regression model (GPR). Incorporating offline model migration and modified random forest regression (mRFR) based on online ensemble learning to estimate SOH, practical problems such as cell inconsistency and online operation are solved [36]. On the other hand, the approach based on neural networks (NN) has been widely used in time series data successfully due to their powerful nonlinear fitting ability, applicability and flexibility. To enhance model performance with time series inputs, contemporary methods predominantly employ Recurrent Neural Networks (RNN), Long Short-Term Memory (LSTM), Gated Recurrent Unit (GRU), and their refined variants, which are particularly adept at processing time series data. [37]. In order to adapt to different operating conditions, improved dynamic RNN and self-adaptive weight particle swarm optimization (SWPSO) algorithm are introduced to improve the estimation accuracy of SOH [38]. Cui et al. [39] design an improved bidirectional gated recurrent unit (IBGRU) network in a combination with an attention mechanism to mitigate the inconsistency of the impact of input data at different time nodes on the results. Sun et al. [40] propose a new SOH estimation method using a directed acyclic graph (DAG) structure based on incremental capacity analysis and GRU, and the minimum mean square error of SOH is reduced to 0.65 %. However, the computation cost of GRU is huger compared to feedforward counterparts like CNN, and in the framework of RNN, it is difficult to rebuild a new model that can obviously outperform GRU. Furthermore, when modeling extended sequences, the scalability of the estimation technique becomes constrained, and the training process is notably prolonged [41,42]. Considering the limitation of long sequences modeling, an attention mechanism is proposed, which can extract features from the

whole sequence by weighting all previous input sequence states [43,44]. Nevertheless, the efficiency of this attention mechanism that only one element can be treated at a time node for capturing long-range dependencies would be affected by inputs data length. Transformer models with encoder-decoder architectures and self-attention mechanism have a global feature learning ability, that is, entire input sequences are trained at the same time, which greatly increases the computational efficiency and reflects relationships among different features appearing in different locations. It is notable that although previous methods have achieved stable and accurate SOH estimation in LIBs, there are still some problems to be addressed. Firstly, in essence, Transformer tends to ignore local feature details, which decreases the discriminability within limited timespan and thus a hybrid network framework called CNN-Transformer has been proposed to estimate SOH [45,46]. Although this model improves the SOH estimation accuracy, it neglects the computational burden and the redundancy of temporal and channel information. Secondly, Transformer-based improved methods focus on reducing the complexity of attention computation and Li et al. [47] have designed the sparse attention mechanisms with only $O(L(\log L)^2)$ memory cost. (L denotes the length of time sequence). However, these methods have a bulk of additional operations beyond attention, which increase the time complexity. According to the current research results, further research on a novel SOH estimation model that can reduce computational burden and redundancy while learning local and long-term dependencies, is a crucial issue in data-driven algorithms.

The main contributions of this study are given as follows:

- (1) In this study, we firstly apply the Mixers structure for SOH estimation of LIBs because it shows significant potential in handling time series problems. Compared with transformer, it removes the encoder-decoder architecture to reduce the computation complexity, and uses feed-forward networks and self-attention mechanisms to capture temporal and channel dependencies, respectively. Li et al. [48] have proved that disentangling the modeling interaction of temporal and channel may improve the estimation performance.
- (2) This article develops a novel SOH estimation framework that combines bidirectional temporal convolutional neural network and Mixers to take the greatest advantage of local and global properties. BTCN is good at collecting local properties hierarchically and learn the dependency between the output and the previous and future input information. Mixers can be used to aggregate global properties through its self-attention mechanisms.
- (3) The HIs extraction method only requires the constant current charging segment, which is conductive to reducing the sampling time and reducing the calculation burden of BMS. After correlation quantification and normalization, the selected features can be directly fed into the Mixers-BTCN model. It is conductive to real-time SOH estimation.
- (4) The Mixers-BTCN method has satisfied estimation accuracy and reliable adaptability performance to adapt to different operating conditions. Additionally, the proposed SOH estimation model can extend to SOH estimation of other lithium-ion batteries by transfer learning, which is proven by mean absolute error (MAE) and root mean square error (RMSE) that are held within 1.68 %.

2. Experimental dataset and features analysis

In practical battery-powered applications, dynamic switching of working conditions and different battery types are primary factors that reduce the adaptability and effectiveness of HIs. Therefore, LiFePO₄ and LiCoO₂ cells are applied to validate the proposed SOH estimation method in this paper.

2.1. Dataset description

The corresponding testing procedures of four batteries that are provided by the Toyota Research Institute (TRI) and the Massachusetts Institute of Technology (MIT), are shown in Table 1. In reference [49], the MIT dataset comprises 124 operational LiFePO₄/graphite cells, each with a rated capacity of 1.1 Ah. These cells undergo cycling through 72 distinct fast charging profiles denoted in the format “C1(Q1)-C2.” This indicates charging at a constant current of C1 until reaching an SOC of Q1 (where Q1 represents the SOC at the point of current switch), followed by charging at C2 until an SOC of 80 % is achieved. Subsequently, the cell undergoes charging at CCCV (1C up to 3.6 V). All cells’ discharging conditions are identical (CCCV, 4C to 2.0 V) and are conducted at temperature of 30 degrees Celsius. Currently, most battery data are got under CCCV charging conditions and are not comparable to MIT dataset when simulating battery degradation under varied fast charging conditions. Fig. 1 shows the measured experimental data of a charging-discharging cycle and the degradation curve of the battery capacity.

The LiCoO₂/graphite prismatic lithium-ion batteries from the Center for Advanced Life Cycle Engineering (CALCE) at the University of Maryland [50,51] are chosen for experiments. The cycling data collection is stopped when the reference capacity decreases to 80 %. The four batteries B35, B36, B37 and B38 undergo the same charging and discharging profile at room temperature (around 25 °C). They are charged with constant current of 0.5C, and the voltage would be sustained after reaching 4.2 V until the current drops to 0.05 A. These cells are discharged at 1C until the terminal voltage drops to 2.7 V. The actual operating curve and capacity decline trend are given in Fig. 2.

In addition, the selection of LFP 18650-20R batteries (B1, B2, B3, B4) with a rated capacity of 2.0 Ah is valuable for studying the robustness of the data-driven method under dynamic temperature. The cells are exposed to a CCCV charging profile, where the current is 0.75C at the CC stage, the upper voltage threshold is 4.2 V, and the terminal current is 0.05 A at the CV stage, followed by the DST discharging stage. Fig. 3 shows the monitored data of voltage, current and temperature in one cycling process.

The experimental test equipment used in this paper and the capacity decline curve obtained are shown in Fig. 4. It includes a CT-4008 (5 V-6 A) tester to charging/discharging batteries, a thermal chamber to control the operating temperature of the battery, and an upper computer to record sensor data under working conditions.

2.2. Charging curves-based extraction of HIs

In order to improve the SOH estimation accuracy, the features highly related to battery degradation should be utilized in the data-driven model. In existing studies, HIs are mainly extracted from the data that can be measured online during the charging-discharging process of LIBs. Typically, the charging protocol is fixed, and thus extracting HIs from the charging data can be easily implemented for SOH estimation, for instance using an incremental capacity (IC) method [52]. In this study, HIs are expressed as follows:

$$HI1 = \frac{\Delta T_1}{\Delta U_i^1}, i = 1, 2, \dots, n \quad (2)$$

$$HI2 = \frac{\Delta T_2}{\Delta U_i^2} \quad (3)$$

$$HI3 = \int_{t_1}^{t_1 + \Delta T_1} I(t) \times U_i^1(t) \times dt \quad (4)$$

$$HI4 = \int_{t_2}^{t_2 + \Delta T_2} I(t) \times U_i^2(t) \times dt \quad (5)$$

where n is the total life cycle number of the battery; ΔT_1 (60s) and ΔT_2 (90s) denote the time interval between the start and end moments, respectively; $U(t)$ and $I(t)$ represent the charging voltage and charging current of equal charging time interval (ECTI) in the i th cycle, respectively; $HI1$ and $HI2$ indicate the ratio of the time interval to voltage change corresponding to different initial voltage; $HI3$ and $HI4$ are the energy in ECTI under CC charging mode. In each charging cycle, the time (t_1 and t_2) should be recorded when the voltage reaches 3.78 V and 3.88 V for the first time, respectively. Taking the charge cycle curve of B35 as an example, Fig. 5(b) shows the feature curves variation at different aging stages when the time interval is 30 s. As shown in Fig. 5 (a), the charging curve corresponding to the peak position in the constant current charging stage is densely distributed. This region is an area where the voltage changes in the equal time range of each cycle are significantly different, and is highly associated to the health status of the battery. Since the specific location of the peak cannot be known in advance, the effectiveness of HIs depends on the selection of initial voltage and time interval.

2.3. Correlation evaluation of lithium-ion battery HIs

As shown in Fig. 6, the starting voltage and the time length are set to (3.76 V, 3.77 V, ..., 3.94 V) and (60s, 90s, ..., 270 s), respectively. The Pearson correlation coefficient $P_{x,y}$ is used to evaluate the association between features and SOH. Positive values of $P_{x,y}$ mean positive correlation, and negative values mean negative correlation. The closer the absolute values of $P_{x,y}$ are to 1, the better the independent variable can explain the dependent variable in regression analysis. Generally, it means that the two variables are strongly correlated when the absolute value of $P_{x,y}$ is greater than 0.8 [53]. In the Eq. (6), σX and σY represent the standard deviation (SD) of X and Y , and $\text{cov}(X, Y)$ represents the covariance of X and Y , respectively.

$$P_{x,y} = \frac{\text{cov}(X, Y)}{\sigma X \sigma Y} \quad (6)$$

It is found that when the initial voltage is located at [3.78, 3.82] V or [3.84, 3.89] V, the correlation coefficient is significantly higher than that of other voltage ranges through experiments results in Fig. 6. Obviously, these regions are exactly where the peaks appear in Fig. 5(b). The starting voltage of 3.88 V and the time segment of 90s achieve the greatest $P_{x,y}$ of 0.996 of all combinations. The combinations [3.78 V, 60s] and [3.88 V, 90s] are chosen to extract HIs in order to meet accuracy and rapidity requirements of SOH estimation. In addition, the absolute values of the correlation coefficients between the HIs and the SOH are all above 0.8 in the voltage range of [3.76, 3.91] V, indicating that HIs are strongly correlated with battery aging in a large voltage range. The strong applicability to different voltage ranges of this method that only using simple extracted features to depict the aging state of cells is confirmed by this encouraging result.

2.4. Feature normalization

We use max-min scaling method to normalize input features into the interval [0,1], which will speed up the training process of the model and reduce the initialization requirement of learning-rate. As shown in followed:

Table 1
Batteries information of MIT dataset.

Cells No.	8	55	62	111
Channel-id	9	27	7	36
Fast-charging profiles	4.8C (80 %) 4.8C	4.0C (13 %) 5.0C	4.8C (80 %) 4.8C	5.6C (19 %) 4.6C
Manufacturer	APR18650M1A			

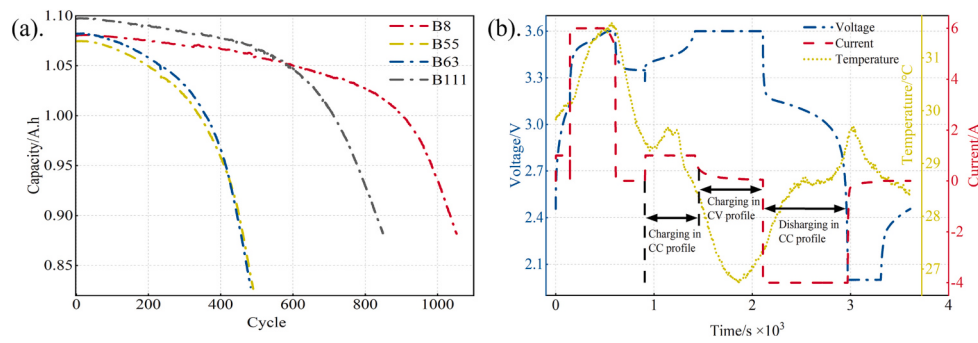


Fig. 1. LFP batteries (a) capacity degradation curves (b) charging-discharging profiles.

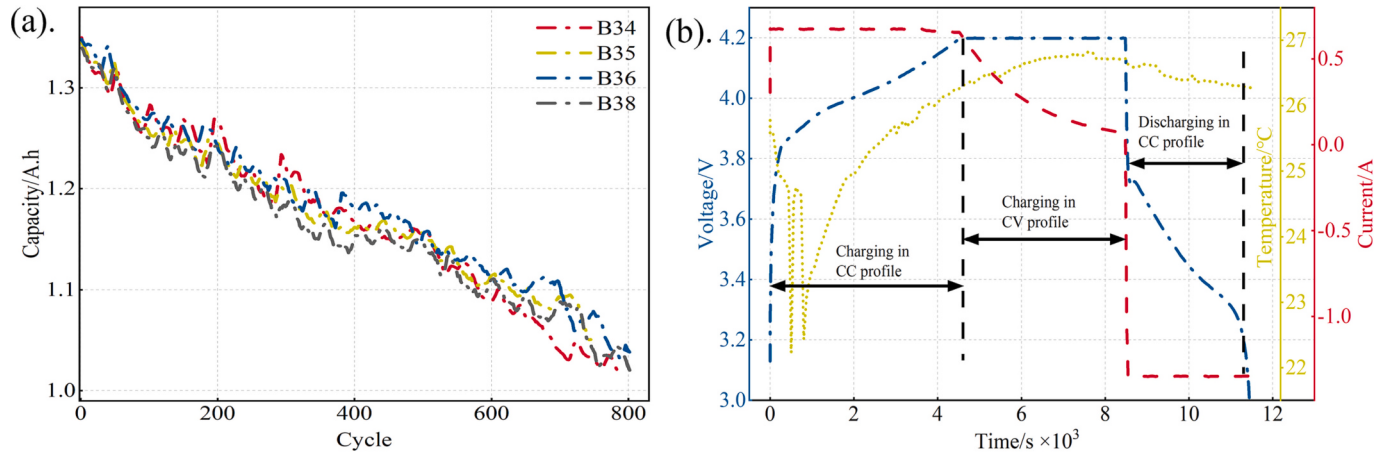


Fig. 2. LCO batteries (a) capacity degradation curves (b) charging-discharging profiles.

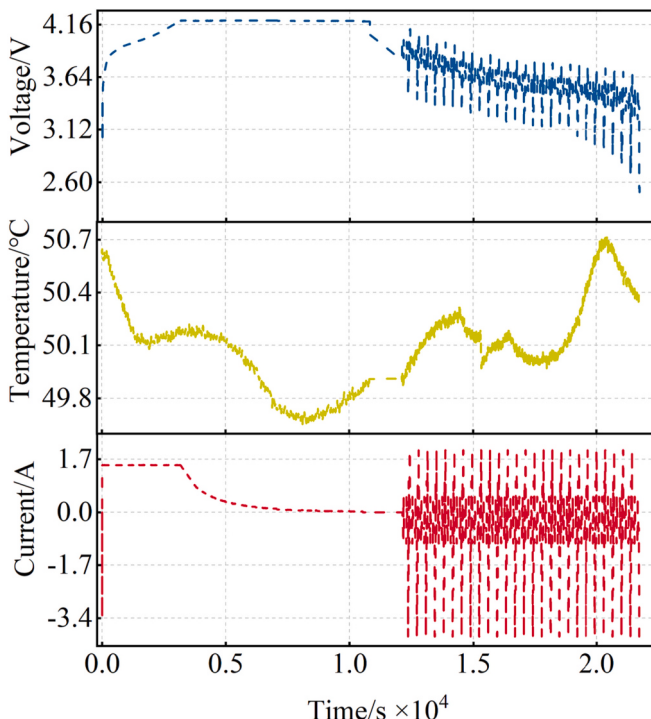


Fig. 3. Charging-discharging profiles of tested batteries.

$$X_{nom} = \frac{X_{in} - X_{min}}{X_{max} - X_{min}} \quad (7)$$

where x_{nom} is the data after normalization, x_{in} is the initial data, x_{min} and x_{max} are the minimum and maximum values of the raw input.

3. Methodology

3.1. Temporal convolution networks

A special type of CNN, temporal convolution network has been successfully applied to the time series data [54]. Differ from the iterative and series structure of GRU, TCN has shown significant potential in parallel computing and has fewer parameters and faster convergence than CNN. In the framework of this network, the convolution operation is achieved by moving across the time axis with a one-dimensional kernel known as temporal convolution. The main characteristics are: (1) The network output is a prediction sequence $\{y_0, y_1, \dots, y_n\}$, which is a nonlinear function of the corresponding input sequence $\{x_0, x_1, \dots, x_n\}$ [55]. (2) Using causal convolutions instead of standard convolutions, and the output at time t is only convolved with data points from t and earlier. Thus, it takes into account historical sequence information while avoiding future information leakage. (3) Dilated convolutions technique is introduced to efficiently avoid problems arising in the process of increasing the receptive field (RF). As seen in Fig. 7, the convolution kernel of size k is dilated by a dilatation factor d wherefore the number of previous steps on which the output at position t depends grows from k_n to k [56]. The RF_n of the TCN can be calculated with the following formula:

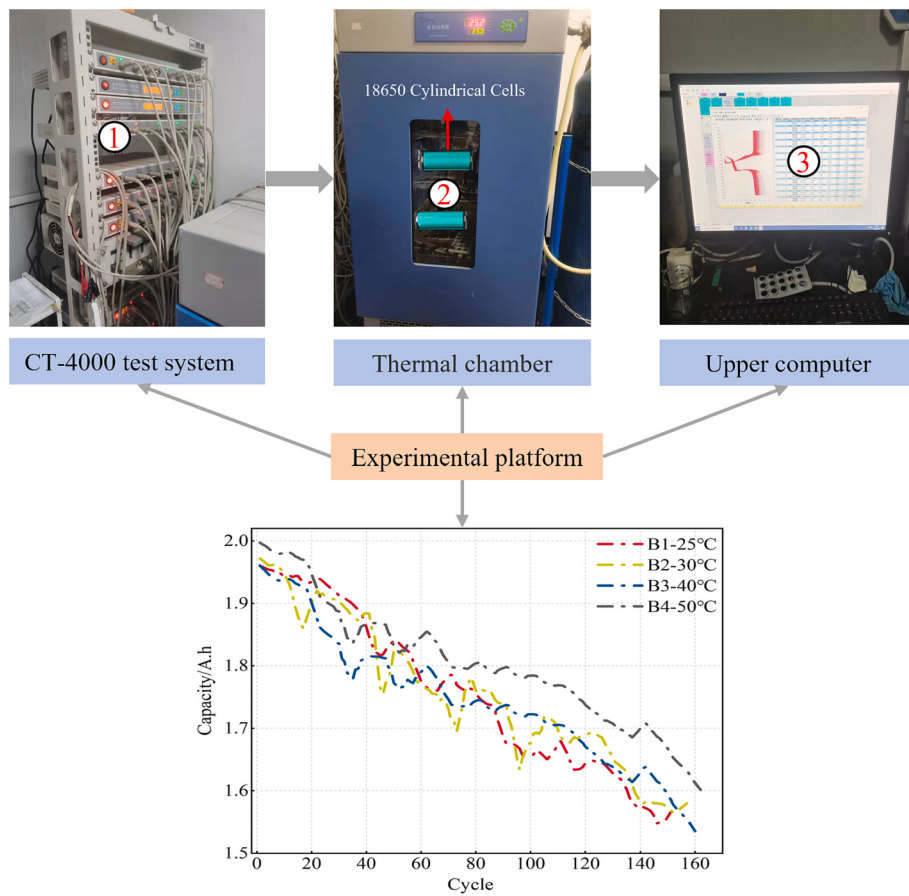


Fig. 4. Experimental equipment and capacity degradation curves of tested batteries.

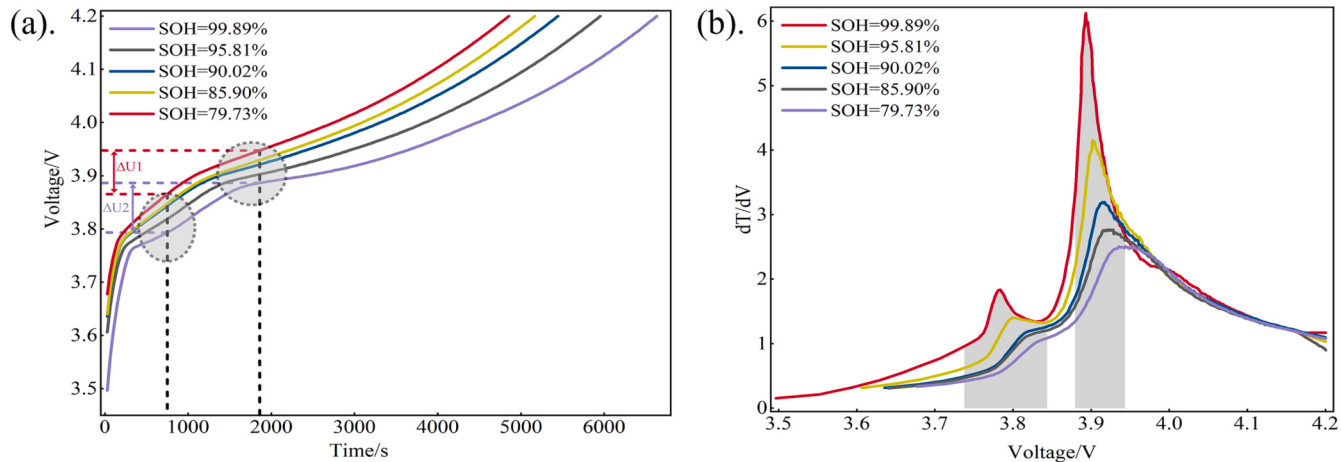


Fig. 5. Curves with cyclic usage (a) CC charging curves (b) dT/dV curves.

$$k = k_n + (d-1) \times (k_n - 1)$$

$$RF_n = RF_{n-1} + (k-1) \times \prod_{i=1}^{n-1} S_i \quad (8)$$

(4) In order to accelerate the convergence speed and keep the stability of the deep TCN network, a skip connection technique is employed, that is, the output of the residual block is a superposition of the feature information of the previous layer and the feature graph of current layer. Given that input-output widths may not be compatible, an additional 1D convolution is used to ensure that addition takes tensors of the same shape.

3.2. Bidirectional temporal convolution networks

In standard TCN structure, utilizing the De-Convolution structure of one-dimensional(1D) fully convolutional network (FCN) to enlarge the size of the output sequence after convolution kernel operation, which is actually the padding of the convolution operation. The padding neurons operation of the convolution is usually applied on the one input side in order to ensure that the input and output of each hidden layer have the same length of time. However, the SOH usually is strongly correlated with both the previous and future input. Therefore, the bidirectional TCN is designed in this paper. The specific structure of the BTEN

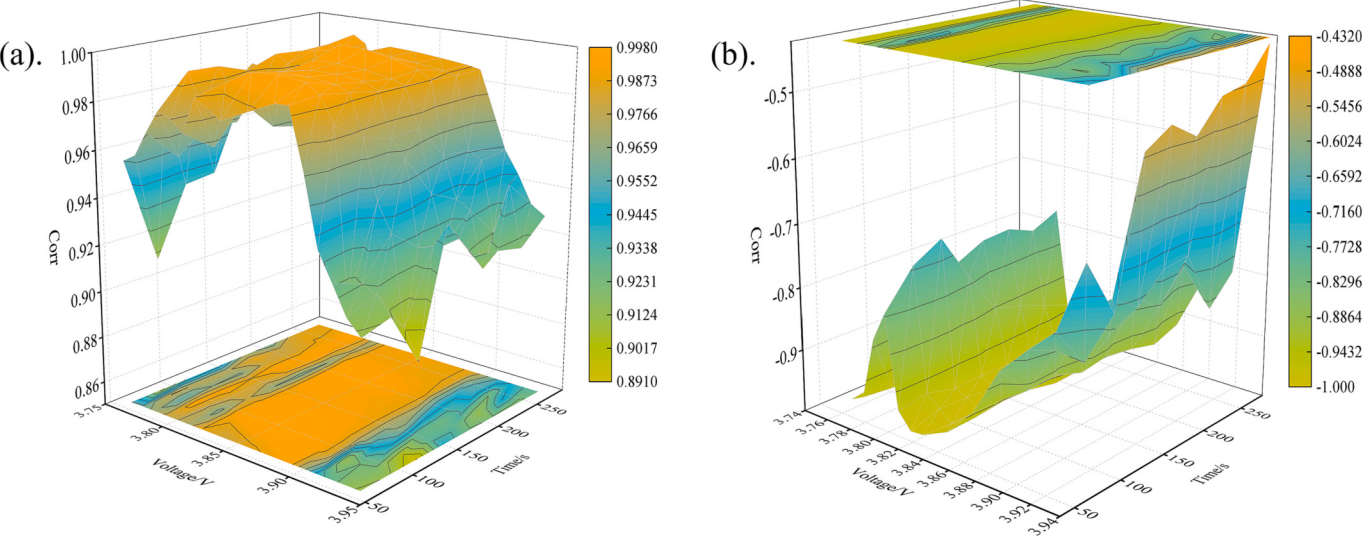


Fig. 6. Three-dimensional surface diagram of Pearson correlation coefficient (a) voltage change in ECTI (b) energy in ECTI.

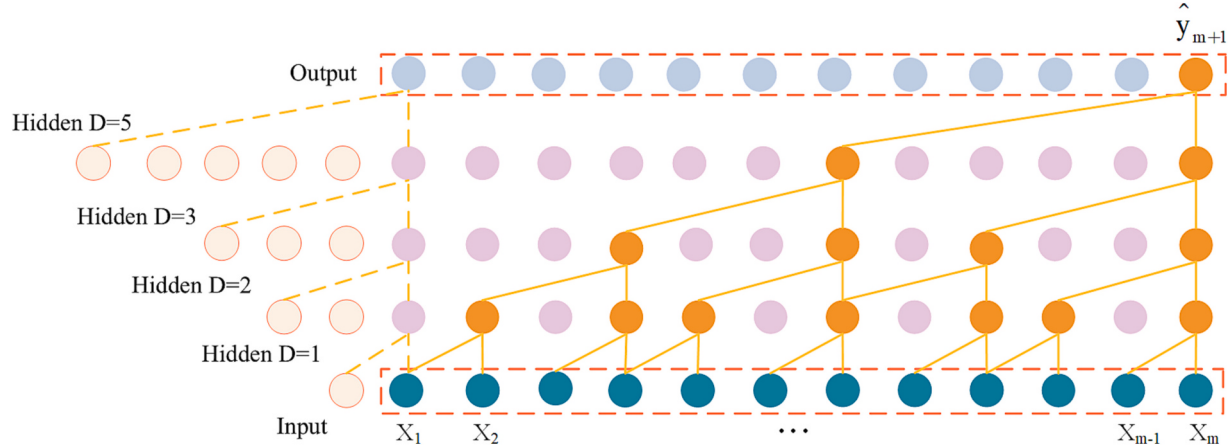


Fig. 7. The causal dilated convolution structure.

contains two TCN layers, one forward propagation layer and one back-propagation layer, which read forward and reverse time sequence information respectively. And it is beneficial to improve the accuracy and robustness of the battery SOH estimation. Looking at the Fig. 8, the two network is symmetrical, meanwhile, the computations are independent of each other.

3.3. Improvement of the BTCN network via Mixers

The SOH estimation of LIBs can be seen as a process of learning the mapping between the observed data made over specific time intervals and SOH. Just like RNNs, the BTCN structure cannot capture long-term dependencies, it shows obvious deficiencies in SOH estimating tasks, which limits the efficiency and accuracy of the prediction model. Abedinia et al. [57] have proposed the attention mechanism based on research about allocating attention resources in the human brain. The key idea is to focus on the information that is more critical to the task at hand among the many inputs, filter out irrelevant information, and thus solve the problem of information overload. It has been proven that the neural network with the attention mechanism improve the efficiency and accuracy of task processing. However, most previous attention mechanisms are applied to the image recognition and text classification, which are not suitable for the SOH estimation.

To this end, Mixers-BTCN used for the SOH estimation is designed in

this paper. BTCN is good at collecting local properties hierarchically and learn the dependency between the output and the previous and future input information. Mixers can be used to aggregate global properties through its self-attention mechanisms. Compared with the Transformer, we remove the decoder to reduce computation complexity and use a linear layer to directly learn the mapping between the learned features from BTCN and the SOH. As shown in Eq. (9), the calculation principle of the redesigned method contains capturing the interaction across channels with a feed-forward network and learning temporal sequences dependency via the self-attention mechanism that is composed of scaled-dot-product attention and multi-head attention, which has revolutionized the implementation of attention mechanisms in recurrence or convolution structure.

$$\begin{aligned} X_h &= \text{Temporal}(X) \\ \tilde{X}_h &= \text{PE}(X_h) \\ X_h^c &= \text{Attention}(\tilde{X}_h, \tilde{X}_h, \tilde{X}_h) \\ X_h^r &= \text{FFN}(\text{LayerNorm}(\tilde{X}_h + X_h^c)) \end{aligned} \quad (9)$$

where *Temporal* denotes the BTCN and *PE* represents the positional encodings. *Attention* represents an attention function and *FFN* is the feed-forward layer. Since there is no recursive operation, the *PE* is applied to provide the input temporal tokens generated in the embedding module with the position information. As shown in following:

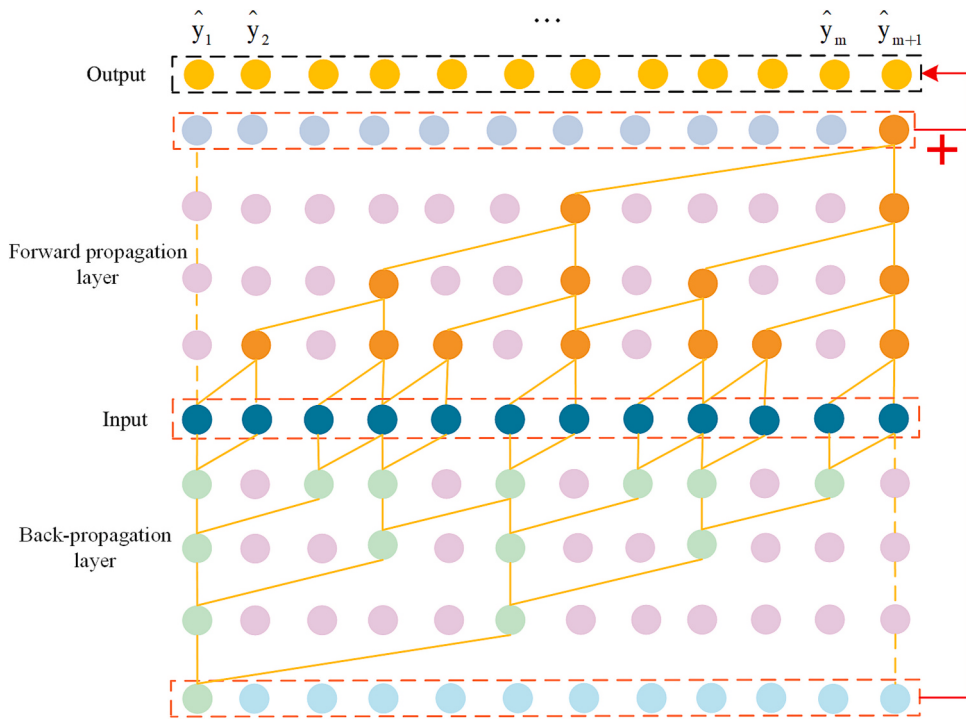


Fig. 8. The bidirectional causal dilated convolution structure.

$$\text{PE}_{(pos,2i)} = \sin\left(\frac{pos}{10000^{\frac{2i}{d_{model}}}}\right) \quad (10)$$

$$\text{PE}_{(pos,2i+1)} = \cos\left(\frac{pos}{10000^{\frac{2i+1}{d_{model}}}}\right) \quad (11)$$

where pos is the position in the temporal sequence and i represents the serial number of the dimension.

In the feed-forward layer, firstly mapping data to the high-dimensional space and then to the low-dimensional space, which makes the ability stronger to express the relationship between the current moment and previous moment input.

$$FFN(X) = \max(0, w_1x + b_1) \cdot w_2 + b_2 \quad (12)$$

The scaled dot-product attention firstly computes a dot product for each query, q , with all the keys, k . It subsequently divides each result by $\sqrt{d_k}$ and proceeds to input the soft-max function, lastly multiplies by values, v :

$$\text{Attention}(Q, K, V) = \text{softmax}\left(\frac{QK^T}{\sqrt{d_k}}\right)V \quad (13)$$

where d_k and d_v represent dimensions, d_k contains the queries vector q and keys vector k , respectively, and d_v contains the values vector v . The equation for the multi-head attention mechanism is built on the above scaled dot-product attention mechanism, as shown below:

$$\text{Multihead}(Q, K, V) = \text{Concat}(\text{head}_1, \dots, \text{head}_h)W^0 \quad (14)$$

$$\text{head}_i = \text{Attention}(QW_i^Q, KW_i^K, VW_i^V), i = 1, \dots, h \quad (15)$$

$$\text{LayerNorm}(X_{\text{embedding}} + \text{self-attention}(Q, K, V)) \quad (16)$$

where Q , K , and V which denote matrices that pack together sets of queries, keys, and values, respectively. W_Q , W_K , and W_V denote projection matrices which are employed to project of the query, key, and value matrices, respectively multiple times. Each head_i represents a single attention function characterized by its own learned projection

matrices. The results of different scaled dot-product attentions are spliced together and then input a linear mapping to generate location information under different subspace.

The BTCN model is improved by introducing Mixers, and the schematic diagram of this SOH estimation method is expressed as Fig. 9. The initialized feature set serve as the input of the proposed model and the output is the battery SOH estimation. The preliminary SOH estimation result is firstly obtained by the BTCN, and then it is optimized by the attention mechanism to get the final SOH estimate. This structure helps the network learn spatial and temporal features separately, which is more efficient and less computationally intensive than learning both features simultaneously.

3.4. Transfer learning

Due to the numerous parameters of the Mixers-BTCN model, a large amount of training data is needed to achieve satisfactory accuracy. In a real-world SOH estimation scenario, collecting battery aging data is time-consuming, and it is unrealistic to train a neural network from scratch for each cell [58]. For lithium-ion batteries of the same specification, despite the existence of performance differences due to varied working conditions, the SOH of LIBs follows a similar nonlinear decline path. In other words, the model parameters trained in the source domain are commonly close to the model parameters in the target domain. Therefore, this paper applies transfer learning to SOH estimation. Following the equation in (17), the Mixers-BTCN model is first trained using the source battery data, and the pre-trained network model is obtained. The resulting θ_s are passed as initial parameters to the target domain where the training data is insufficient, and then θ_s are retrained to learn the difference between the target battery and the source battery. Similarly, the target network parameters θ_t are derived by minimizing the mean square error of SOH estimation.

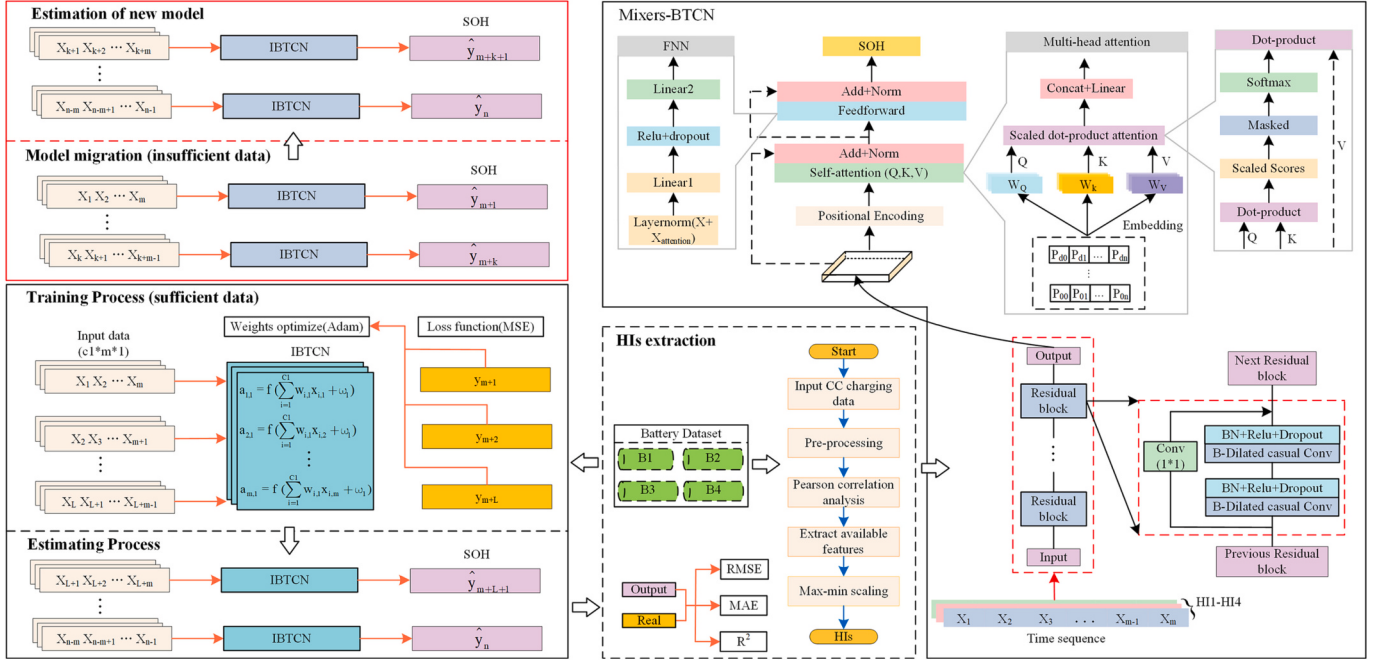


Fig. 9. The schematic diagram of the proposed SOH estimation method.

$$\theta_s = \operatorname{argmin} \frac{1}{n} \sum_{i=1}^n (\hat{y}_i^s - y_i^s)^2$$

$$\theta_t = \operatorname{argmin} \frac{1}{m} \sum_{i=1}^m (\hat{y}_i^t - y_i^t)^2$$

where \hat{y}_i^s is the estimation value and y_i^s is the reference value of SOH. In the training process of target task model, the number of iterations required to realize parameter identification is less, which contributes to mitigate the quantity of data and calculation complexity.

4. Experimental results and discussion

This section predominantly focuses on assessing the performance of the SOH estimation model. We employ two data training strategies to verify the efficacy of the proposed SOH estimation approach, using the cell datasets described in Section 2 and the well-chosen health indicators. The hardware platform is a PC equipped with 64-bit Microsoft Windows 11. The device processor is Intel(R) core (TM) i7-12700 and the total RAM is 16G. The python 3.6.5 is used as the software platform, and all the experimental are conducted on the deep learning framework torch 1.10.2.

4.1. The evaluation criteria

In this paper, three statistical indicators: root mean square error (RMSE), mean absolute error (MAE), and coefficient of determination (R^2) are employed to analyze the performance of the suggested model. MAE is used to measure the average deviation of the observed value and the true value [59]. RMSE indicates the prediction stability of the proposed method. It should be noted that the smaller R^2 values, the lower fitting accuracy of the observations by the regression model is. The definitions of these evaluation metrics are given in the following.

$$RMSE = \sqrt{\frac{1}{n} \sum_{i=1}^n (y_i - \hat{y}_i)^2} \times 100\% \quad (18)$$

$$MAE = \frac{1}{n} \sum_{i=1}^n |y_i - \hat{y}_i| \times 100\% \quad (19)$$

$$R^2 = 1 - \frac{\sum_{i=1}^n (y_i - \hat{y}_i)^2}{\sum_{i=1}^n (y_i - \bar{y})^2} \quad (20)$$

where n denotes the total number of input samples, y_i , \hat{y}_i and \bar{y} denote the model-estimated SOH value, the true SOH value and the average SOH value of all cycles, respectively.

4.2. SOH estimation results based on LCO cells

This subsection will assess the performance of the SOH estimator by using four LiCoO₂ prismatic cells from the CALCE dataset. In the validation procedure, the first 50 % of each battery's cycle data is adopted as the training set, while the rest data up to the EOL is used as the test set. The EOL is set to the 80 % of battery's initial capacity. The estimation results of the proposed Mixers-BTCN estimation model are presented in Fig. 10. It is apparent that the estimated SOH curve agrees well with the reference profile. In order to more clearly illustrate the estimation errors, Table 2 shows the evaluation criteria of corresponding forecasted SOH of four cells, B34, B36, B37 and B38, respectively. Looking at the Table 2, MAEs of the SOH estimation are not more than 1 %, and most are within 1 %. SOH prediction errors are greatest for the B37, and the MAE is 1.34 % and RMSE is 1.28 %. For other three batteries, it can be found that the RMSE distribution are located in the lower range of 0.71 % ~ 0.99 %, meanwhile, R^2 measured is not less than 0.92. These results all prove the validity of the Mixers-BTCN proposed in this study.

4.3. SOH estimation based on LFP batteries with fast-charging protocol

Most types of battery dataset are tested in fixed CCCV charging mode, but the cycle life is associated to charging and discharging current. The specific reason is that the temperature variation is affected by the working current, which in turn affects the internal impedance, and SOH is a function of the internal impedance. In the MIT dataset, varied

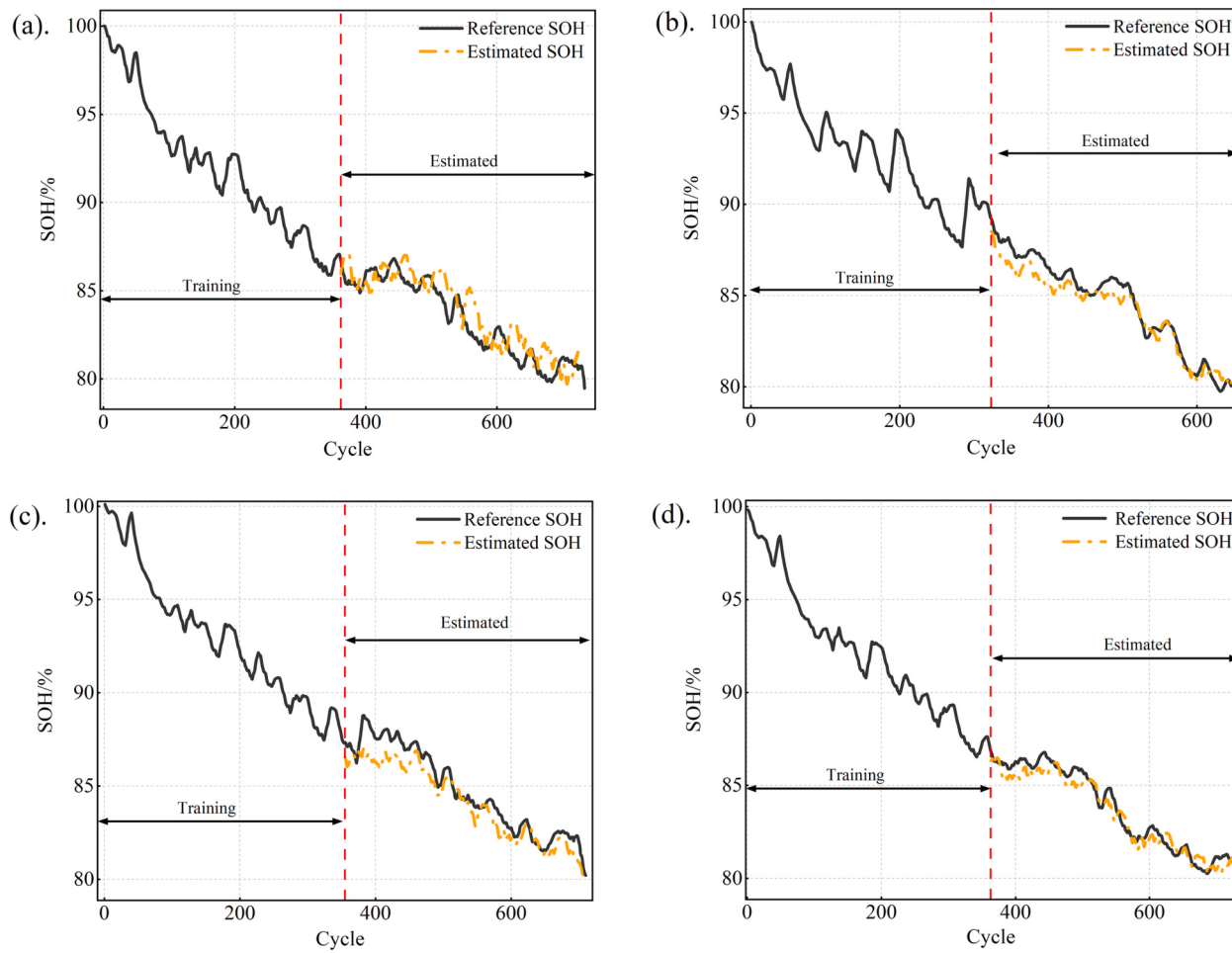


Fig. 10. The SOH estimation results (a) B34 (b) B36 (c) B37 (d) B38.

Table 2
MAE, RMSE and R^2 of SOH estimation of LCO cells.

Cell	MAE (%)	RMSE (%)	R^2
B34	0.82	0.91	0.926
B36	0.96	0.99	0.982
B37	1.34	1.28	0.907
B38	0.53	0.71	0.954

charging conditions as a major factor affecting battery degradation rates, resulting in LFP cells showing different cycle lives. Battery life below 500 cycles is considered short life, and vice versa is long life.

In this perspective, the following experiments are carried out to validate the application prospects of the proposed method on LFP lithium-ion batteries in fast charging mode. Four cells, B8 (long life), B55(short life), B62(short life) and B111(long life), are used, in which B8 and B62 are one-step charging strategy, and the other two cells are two-step charging. The first 50 % of the battery data is used as the training sets and the remaining data is used as the testing set. According to the Fig. 11, the estimated SOH decline curve significantly aligns with the real SOH. As can be seen from the Table 3, the average values of RMSE and MAE are 0.448 % and 0.44 %, respectively. Moreover, the RMSE value of all the tested cells do not exceed 0.82 %, while the R^2 values are all above 0.924. These results turn out that the proposed SOH estimation model has the ability to accurately estimate the SOH of LiFePO₄ batteries in fast charging model.

4.4. Comparison of experimental results of different algorithms

In order to evaluate the estimation performance of the proposed Mixers-BTCN model, it was compared with three data-driven models, TCN-LSTM, BTCN, and TCN, while ensuring the same dataset, training strategy and evaluation criteria. Such so, in following experiments, two long life batteries, B8, and B111 were utilized to verify the estimation performance of the Mixers-BTCN method.

Fig. 12 (a) and (b) present the SOH estimation results of battery #8 and #111 under different algorithms, and Fig. 12 (c) and (d) display the relative estimation errors of the two batteries individually. It can be noted that the SOH errors of Mixers-BTCN are less than 1 %, while the errors of other three strategies are within 2 %, 4 %, and 5 %, respectively. Compared with the estimated results of Mixers-BTCN, it can be observed from Table 4 that the estimated error of the TCN-LSTM model is only slightly enlarged, and the average RMSE and MAE are 0.96 % and 0.77 % respectively. For other two algorithms, the MAE is 2.15 % and 1.98 %, respectively, and the RMSE can be limited to the level lower than 2.45 %. As for Mixers-BTCN, it can be found that the RMSE distribution of two cells is in the lower range of 0.26 % ~ 0.59 %, the maximum value of MAE is only 0.43 %, and the measured R^2 is larger than 0.99. In conclusion, satisfied performance is achieved regarding the SOH estimation accuracy by using the Mixers-BTCN model.

As shown in Table 5, there are four evaluation indicators for the computational cost and speed: training time, testing time, parameters and storage size. The training time represents the model training efficiency. The storage size and parameters denote the model computational complexity. We can see that the Mixers-BTCN model has no

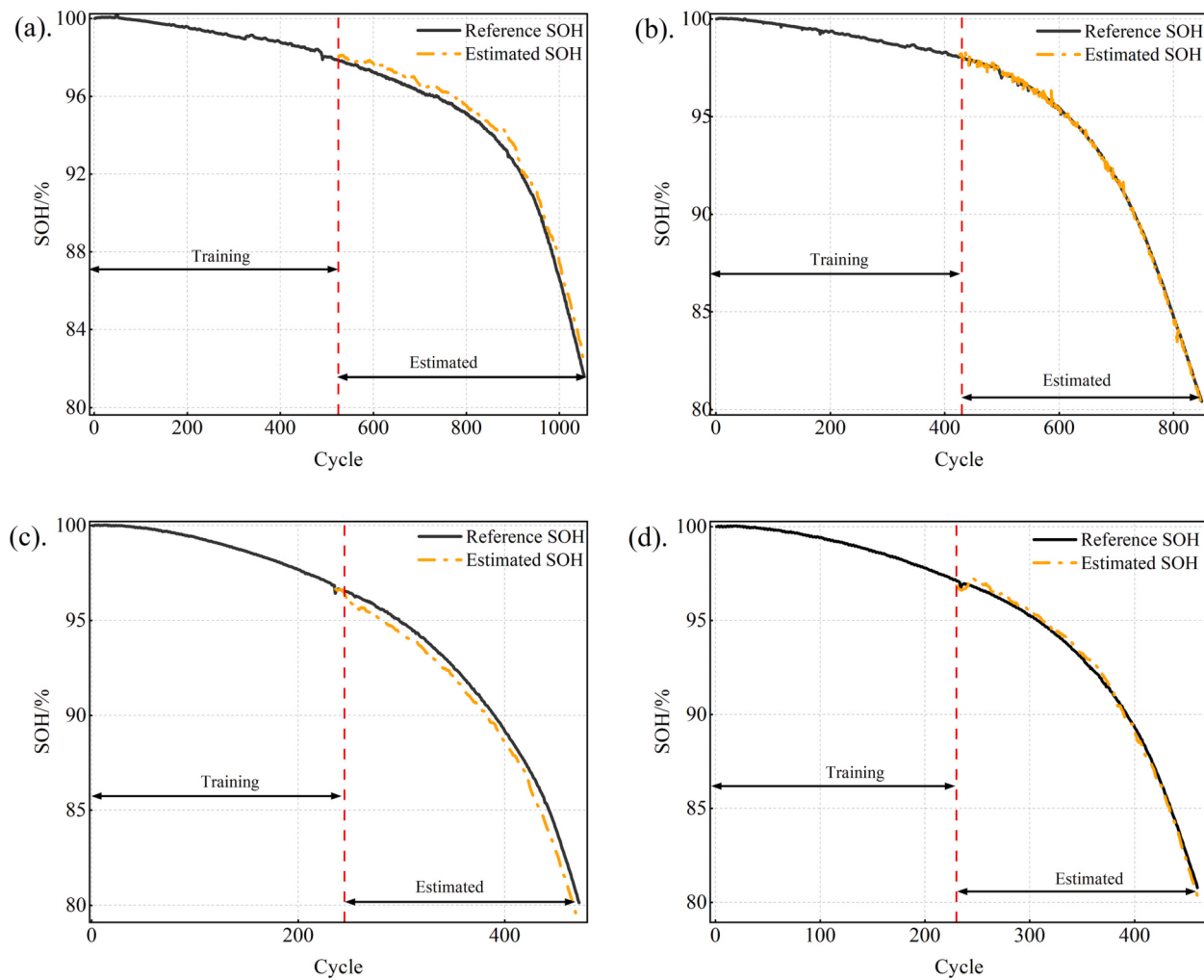


Fig. 11. The SOH estimation results (a) B8 (b) B111 (c) B55 (d) B62.

Table 3
MAE, RMSE and R^2 of SOH estimation of LFP cells.

Cell	MAE (%)	RMSE (%)	R^2
B8	0.73	0.82	0.924
B55	0.09	0.13	0.996
B62	0.58	0.66	0.971
B111	0.16	0.18	0.998

obvious advantages in training time and storage size compared to the two single models, TCN and BTCN. Additional, TCN-LSTM spend much more training time than Mixers-BTCN. This is due to the more complex structure and more parameters. All these data-driven methods can be implemented online testing in a short test time, but the model proposed in this paper has better SOH estimation accuracy.

A comparative analysis of the proposed method versus current state-of-the-art techniques is presented in Table 6. Observably, with the exception of results from the Vision Transformer Network, CNN-Transformer, and MVIP-Trans, the RMSE of our proposed method outperforms that of other SOH estimation algorithms. Similar to the analytical view of Mixers-BTCN, MVIP-Trans and CNN-transformer aim to integrating the benefits of transformer and CNN architectures to learn global and local features from multiple perspectives, enabling comprehensive information perception. When comparing with the SOH estimation results from the MVIP-Trans model, the RMSE of the Mixers-BTCN experienced an 18 % surge, rising from 0.5 % to 0.59 %. This

suggests that the Mixers-BTCN model falls short in terms of SOH estimation accuracy. However, the CNN-transformer focuses on estimation accuracy while ignoring the computational complexity and the over-concentration problem of the attention block. In comparison, our proposed method refines the transformer structure, eliminating the encoder-decoder architecture to lighten the model's weight. By employing feed-forward networks and self-attention mechanisms, it efficiently captures temporal and channel dependencies, thereby reducing redundancy. In addition, by introducing the Mixers framework, a novel analytical perspective is provided for the study of SOH estimation based on deep learning models. It is worth noting that the results of the proposed method are obtained under conditions where only partial charging curves are available, which is well suited for practical SOH estimation due to the difficulty in obtaining complete charging data. In summary, the proposed method has ideal SOH estimation accuracy, and has the foreseeable potential for further study and development in the SOH estimation of LIBs.

4.5. SOH estimation of batteries at different ambient temperature

The validity of the proposed SOH estimation approach may depend on the ambient temperature, since temperature is a major factor affecting battery aging. Specifically, the activation energy of the internal materials inside the battery will increase with the increase of temperature, and thus the capacity degradation trend and the actual usable capacity are different at varied temperatures. In this case, the model

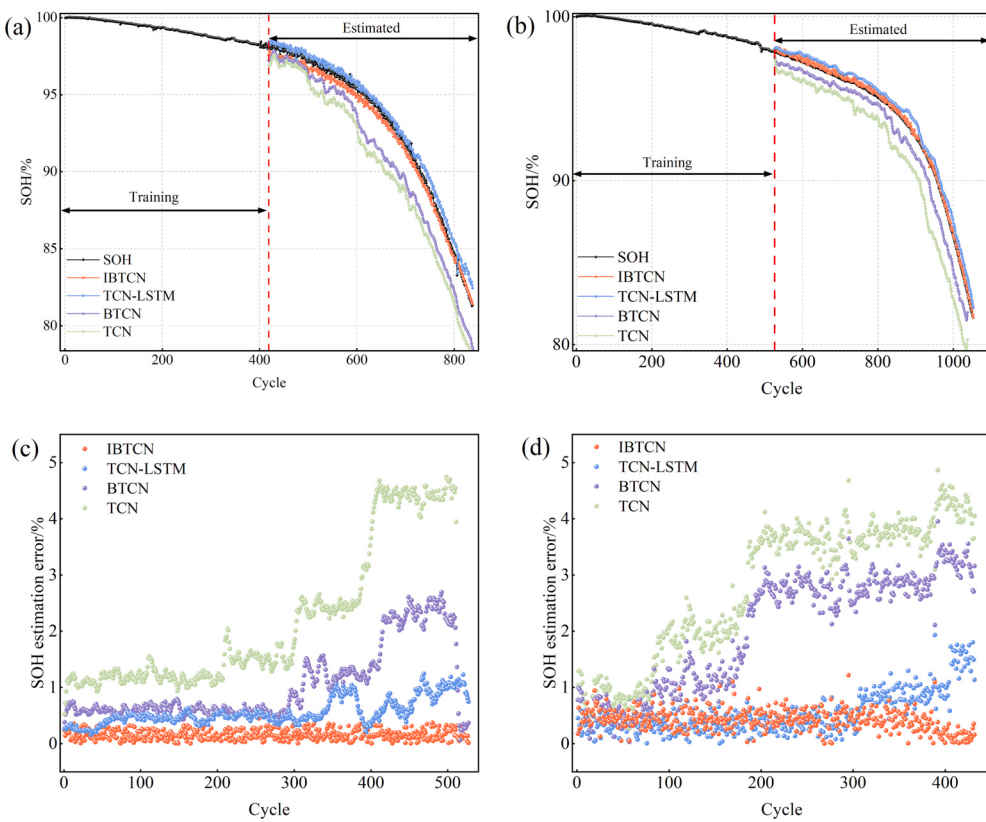


Fig. 12. The SOH estimation results with different algorithms (a) SOH estimation results of B8 (b) SOH estimation results of B111 (c) the relative estimation error of B8 (d) the relative estimation error of B111.

Table 4
Evaluation metrics of SOH estimation for different algorithms.

Cell	Voltage range	MAE (%)	RMSE (%)	R ²
B8	Mixers-BTCN	0.21	0.26	0.994
	TCN-LSTM	0.93	1.2	0.981
	BTCN	1.53	1.77	0.792
	TCN	2.15	2.45	0.769
B111	Mixers-BTCN	0.43	0.59	0.995
	TCN-LSTM	0.62	0.75	0.993
	BTCN	1.62	1.86	0.788
	TCN	1.98	2.34	0.779

Table 5
The comprehensive evaluation of our proposal method and the comparison methods.

Method	Training time (s)	Testing time (s)	Storage size (MB)	Parameters (Thousands)
Mixers-BTCN	590	0.17	0.72	4.96
TCN-LSTM	1467	0.22	0.98	6.2
BTCN	420	0.13	0.33	2.96
TCN	408	0.15	0.32	2.88

parameters obtained after training are also different. Therefore, aging data of lithium-ion batteries tested at 25 °C, 30 °C, 40 °C and 50 °C are used to verify whether the effectiveness of the model can maintain at different temperatures [65–68].

During the validation procedure, the SOH is computed using the first 50 % cycles as the training set, and the remaining data as the testing set. The data used is set to the data before the battery loses 20 % of its initial capacity. Fig. 13 exhibits the results of SOH estimation at different

Table 6
Comparison of the recent publications and our proposed method for SOH estimation results.

Method	Authors	Metric	Error
GPR	Goh et al. [35]	RMSE	1.63 %
CNN-Transformer	Gu et al. [45]	RMSE	0.32 %
SSA-Elman	Guo et al. [53]	RMSE	0.97 %
TCN	Bockrath et al. [54]	RMSE	1.0 %
PSO-LSTM	Gong et al. [60]	RMSE	0.78 %
IPSO-BPNN	Ma et al. [61]	RMSE	0.77 %
MVIP-Trans	Bai et al. [62]	RMSE	0.5 %
Vision transformer networks	Chen et al. [63]	RMSE	0.55 %
Transformer	Luo et al. [64]	RMSE	0.64 %
Mixers-BTCN	Gao et al.	RMSE	0.59 %

temperatures, and the estimated errors are reported in Table 7. The estimated error for the B3 is slightly larger than that of the other three batteries, with MAE and RMSE of 1.38 % and 1.71 %, respectively. The MAEs of the other three batteries ranged from 0.78 % to 1.19 %, while the RMSE typically ranged from 0.87 % to 1.27 %. The minimum R² is still as high as 0.786. The experimental results show that the proposed model has good applicability to different ambient temperatures.

4.6. SOH estimation based on transfer learning

In this section, the model is trained using all cycle data from cell #1, and the remaining B2, B3, and B4 batteries with ambient temperature of 30 °C, 40 °C, and 50 °C, respectively, are combined with transfer learning to validate the robustness of the training model. Since the calculation process of LSTM is incompatible with this estimate scheme [51], the method proposed in this paper is more capable of extending the application. The estimation results and error curves at different temperature are shown in Fig. 14. It is notable that the mean transfer

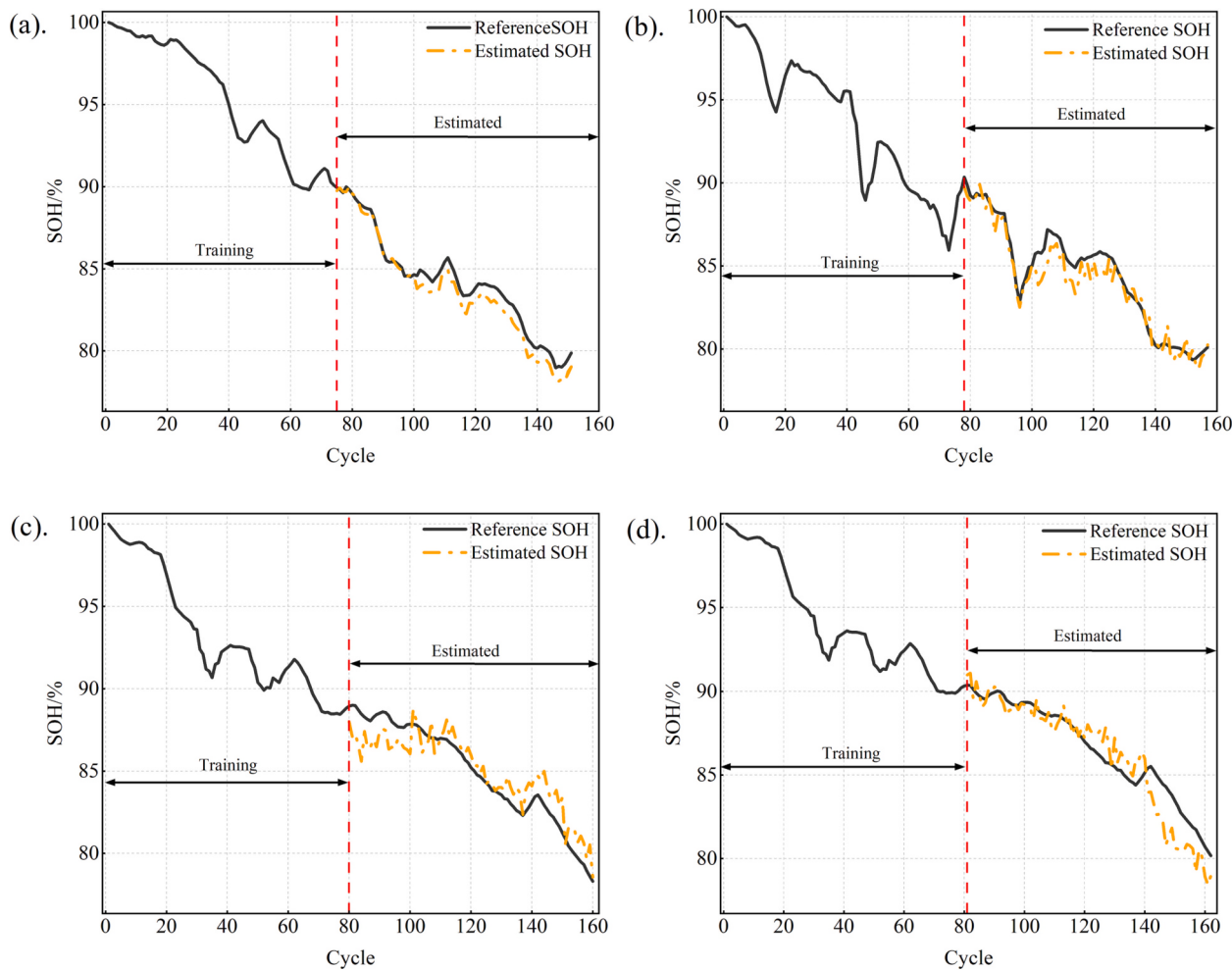


Fig. 13. The SOH estimation results (a) B1 (b) B2 (c) B3 (d) B4.

Table 7

MAE, RMSE and R^2 of SOH estimation under different ambient temperature.

Cell	MAE (%)	RMSE (%)	R^2
B1	0.78	0.87	0.924
B2	1.19	1.27	0.786
B3	1.38	1.71	0.841
B4	1.05	1.2	0.792

training time is around 0.06 h, which is much smaller than the time of 0.28 h for the source task based on the complete data.

The results of trials using various batteries as testing sets are summarized in Table 8. It is worth noting that the estimated error of B2 is smaller than that of B3 and B4, indicating that the closer the working temperature is, the higher the transfer learning accuracy is. As can be seen from Table 8, the maximum error occurs when the working temperature is 50 °C, with MAE of 1.49 % and RMSE of 1.68 %. Nevertheless, this is still within an acceptable error range. Therefore, the pre-trained model can be transferred to estimate the SOH of another similar battery at various environment temperatures, thus reducing the training time.

5. Conclusion

In this paper, the Mixers-BTCN is proposed for SOH estimation of lithium-ion batteries. Specifically, we've designed the BTCN structure, which comprises two symmetrical TCN layers. Notably, the

computations within these layers operate independently of one another. It is beneficial to improve the accuracy and robustness of the battery SOH estimation. Mixers capture temporal and channel dependencies using a self-focused mechanism and a feedforward network, respectively, to help distinguish the impact of data at different time points on output and reduce the redundancy of temporal and channel information.

The Mixers-BTCN takes the greatest advantage of local and global properties of input features to estimate SOH of lithium-ion batteries. The validation scheme is performed using different types of LIBs from MIT and CALCE datasets containing fast charging and dynamic discharging scenarios. The simulation results indicate that the proposed SOH estimation model has great adaptivity and accuracy for different types of lithium-ion batteries, with RMSEs and MAEs both less than 2.34 % and R^2 greater than 0.769. Moreover, the introduction of transfer learning technology proves the robustness of the proposed SOH estimation model. The R^2 of all tested batteries is greater than 0.836 when the pre-trained model is transferred to the same type of battery at various ambient temperature, which is not only reduces the training time, but also makes it easier to cope with the dynamic temperature situation in practical applications. Although the proposed model has great performance in SOH estimation accuracy and model transfer learning, there are several limitations in the present work that need to be addressed in future work. Firstly, the proposed method pays attention to the estimation accuracy, but increases the calculation burden. Compared with typical LSTM or TCN models, the Mixers-BTCN model is not competitive in training time and number of parameters, indicating that the model has higher computational complexity. Secondly, during the charging

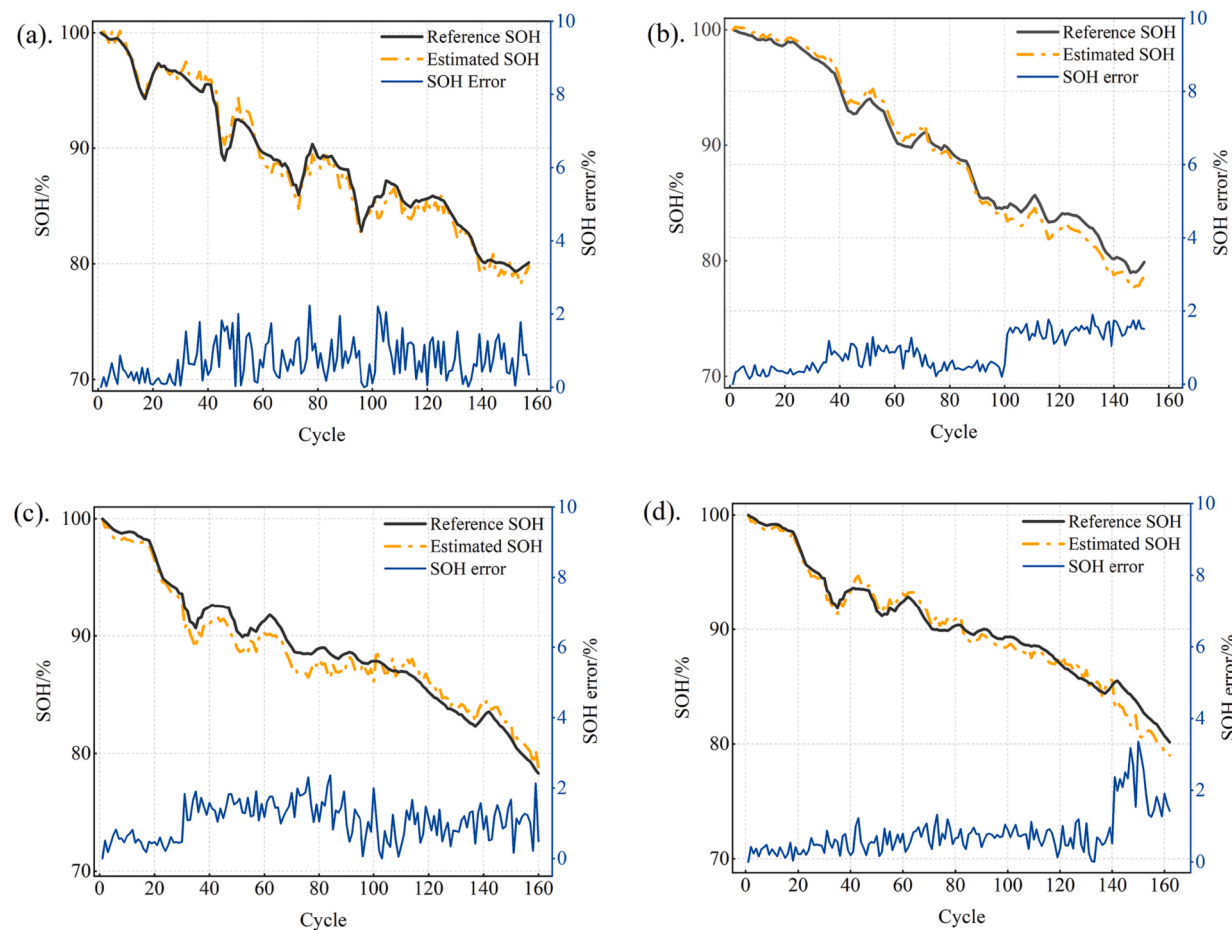


Fig. 14. The SOH estimation results with transfer learning (a) B1 (b) B2 (c) B3 (d) B4.

Table 8

MAEs, MSEs and R² of SOH estimation based on transfer learning.

Cell	MAE (%)	RMSE (%)	R ²
B1	0.73	0.83	0.937
B2	0.85	0.97	0.906
B3	1.22	1.58	0.836
B4	1.49	1.68	0.882

process, if the initial charging voltage exceeds 3.9 V and the initial SOC surpasses 20 %, it poses challenges to extracting HIs that are closely correlated with the degradation of SOH. Heavily incomplete discharging may even result in subsequent HIs extraction failure. Thirdly, the dynamic charging current and temperature will cause the mitigation and distortion of the voltage curve, reducing the predictive ability of the proposed method. In the future work, we should consider reducing the calculation cost of the proposed model on the premise of ensuring the estimation accuracy. In addition, battery datasets of heavily incomplete discharging should be used to evaluate the robustness of the model. Finally, it is significant to reduce the training time and online estimation time of SOH models.

CRediT authorship contribution statement

Jingyi Gao: Conceptualization, Methodology, Software. **Dongfang Yang:** Data curation, Writing-Original draft preparation, Visualization, Investigation. **Kai Wang:** Supervision, Writing-Reviewing and Editing. **Licheng Wang and Zhaotong Li:** Software, Validation. **Shi Wang:** Writing-Reviewing and Editing.

Declaration of competing interest

The authors declare that they have no known competing financial interests or personal relationships that could have appeared to influence the work reported in this paper.

Data availability

Data will be made available on request.

Acknowledgements

This research was funded by the Guangdong Provincial Key Lab of Green Chemical Product Technology (GC202111), Zhejiang Province Natural Science Foundation (No. LY22E070007), the National Natural Science Foundation of China (62133007) and National Natural Science Foundation of China (No. 52007170).

References

- [1] Y.H. Li, K. Li, X. Liu, X. Li, L. Zhang, B. Rente, et al., A hybrid machine learning framework for joint SOC and SOH estimation of lithium-ion batteries assisted with fiber sensor measurements, *Appl. Energy* 325 (2022).
- [2] S. Son, S. Jeong, E. Kwak, J.H. Kim, K.Y. Oh, Integrated framework for SOH estimation of lithium-ion batteries using multiphysics features, *Energ. Environ. Sci.* 15 (2022).
- [3] N. Ma, H. Yin, K. Wang, Prediction of the remaining useful life of supercapacitors at different temperatures based on improved long short-term memory, *Energies* 11 (2) (2023) 38.
- [4] Z.L. Wang, X.Y. Zhao, H. Zhang, D. Zhen, F.S. Gu, A. Ball, Active acoustic emission sensing for fast co-estimation of state of charge and state of health of the lithium-ion battery, *J. Energy Storage* 64 (2023).

- [5] P. Ma, S. Cui, M. Chen, S. Zhou, K. Wang, Review of family-level short-term load forecasting and its application in household energy management system, *Energies*. 16 (15) (2023) 5809.
- [6] X. Sun, Y. Zhang, Y. Zhang, L. Wang, K. Wang, Summary of health-state estimation of lithium-ion batteries based on electrochemical impedance spectroscopy, *Energies*. 16 (15) (2023) 5682.
- [7] Z. Yi, Z. Chen, K. Yin, L. Wang, K. Wang, Sensing as the key to the safety and sustainability of new energy storage devices, *Prot. Contr. Modern Power Syst.* 8 (1) (2023) 27.
- [8] C.Y. Zhang, C.X. Cao, R.Q. Chen, J.H. Jiang, Three-leg quasi-Z-source inverter with input ripple suppression for renewable energy application, *Energies*. 16 (11) (2023) 4393.
- [9] N. Ma, D.F. Yang, S. Riaz, L.C. Wang, K. Wang, Aging mechanism and models of supercapacitors: a review, *Technologies*. 11 (2) (2023) 38.
- [10] H. Sun, J. Sun, K. Zhao, L. Wang, K. Wang, Data-driven ICA-bi-LSTM-combined lithium battery SOH estimation, *Math. Probl. Eng.* 2022 (2022) 9645892.
- [11] F.K. Wang, Z.E. Amogne, J.H. Chou, C. Tseng, Online remaining useful life prediction of lithium-ion batteries using bidirectional long short-term memory with attention mechanism, *Energy*. 254 (2022).
- [12] X.B. Han, L.G. Lu, Y.J. Zheng, X.N. Feng, Z. Li, J.Q. Li, et al., A review on the key issues of the lithium ion battery degradation among the whole life cycle, *Etransportation*. 1 (2019).
- [13] S.Y. Li, X.Y. Jin, Y. Xuan, X.Y. Zhou, W.H. Chen, Y.X. Wang, et al., Enhancing the locality and breaking the memory bottleneck of transformer on time series forecasting, *Adv. Neur In.* 32 (2019).
- [14] Y. Guo, P. Yu, C. Zhu, K. Zhao, L. Wang, K. Wang, A state-of-health estimation method considering capacity recovery of lithium batteries, *Int. J. Energy Res.* 46 (15) (2022) 23730–23745.
- [15] F.J. Wang, Z.B. Zhao, Z. Zhai, Z.G. Shang, R.Q. Yan, X.F. Chen, Explainability-driven model improvement for SOH estimation of lithium-ion battery, *Reliab. Eng. Syst. Saf.* 232 (2023).
- [16] H.H. Pan, Z.Q. Lu, H.M. Wang, H.Y. Wei, L. Chen, Novel battery state-of-health online estimation method using multiple health indicators and an extreme learning machine, *Energy*. 160 (2018) 466–477.
- [17] K. Wang, L. Li, Y. Lan, P. Dong, G. Xia, Application research of chaotic carrier frequency modulation technology in two-stage matrix converter, *Math. Probl. Eng.* 2019 (2019) 2614327.
- [18] M. Dubarry, C. Truchot, B.Y. Liaw, Synthesize battery degradation modes via a diagnostic and prognostic model, *J. Power Sources* 219 (2012) 204–216.
- [19] D. Ansean, M. Dubarry, A. Devie, B.Y. Liaw, V.M. Garcia, J.C. Viera, et al., Fast charging technique for high power LiFePO₄ batteries: a mechanistic analysis of aging, *J. Power Sources* 321 (2016) 201–209.
- [20] M. Zhang, Y.S. Liu, D.Z. Li, X.L. Cui, L.C. Wang, L.W. Li, et al., Electrochemical impedance spectroscopy: a new chapter in the fast and accurate estimation of the state of health for lithium-ion batteries, *Energies*. 16 (4) (2023) 1599.
- [21] Y. Liu, L. Wang, D. Li, K. Wang, State-of-health estimation of lithium-ion batteries based on electrochemical impedance spectroscopy: a review, *Prot. Contr. Modern Power Syst.* 8 (2023) 41.
- [22] L. Cai, J.H. Meng, D.I. Stroe, J.C. Peng, G.Z. Luo, R. Teodorescu, Multiobjective optimization of data-driven model for lithium-ion battery SOH estimation with short-term feature, *IEEE T Power Electr.* 35 (11) (2020) 11855–11864.
- [23] L. Chen, W. Yu, G. Cheng, J. Wang, State-of-charge estimation of lithium-ion batteries based on fractional-order modeling and adaptive square-root cubature Kalman filter, *Energy*. 271 (2023) 127007.
- [24] C. Wang, S.L. Wang, J.Z. Zhou, J.L. Qiao, X. Yang, Y.X. Xie, A novel back propagation neural network-dual extended Kalman filter method for state-of-charge and state-of-health co-estimation of lithium-ion batteries based on limited memory least square algorithm, *J. Energy Storage* 59 (2023).
- [25] Z.X. Li, S.Y. Shen, Z. Zhou, Z.D. Cai, W.M. Gu, F.Y. Zhang, Novel method for modelling and adaptive estimation for SOC and SOH of lithium-ion batteries, *J. Energy Storage* 62 (2023).
- [26] X. Shu, G. Li, J.W. Shen, Z.Z. Lei, Z. Chen, Y.G. Liu, An adaptive multi-state estimation algorithm for lithium-ion batteries incorporating temperature compensation, *Energy*. 207 (2020).
- [27] M. Zhang, K. Wang, Y.-t. Zhou, Online state of charge estimation of lithium-ion cells using particle filter-based hybrid filtering approach, *Complexity* 2020 (2020), 8231243.
- [28] C. Liu, D. Li, L. Wang, L. Li, K. Wang, Strong robustness and high accuracy in predicting remaining useful life of supercapacitors, *APL Mater.* 10 (6) (2022), 061106.
- [29] X. Hu, L. Xu, X. Lin, M. Pecht, Battery lifetime prognostics, *Joule*. 4 (2) (2020) 310–346.
- [30] X.F. Yu, Y.K. Li, X.A. Li, L.C. Wang, K. Wang, Research on outdoor mobile music speaker battery management algorithm based on dynamic redundancy, *Technologies*. 11 (2) (2023) 60.
- [31] M. Zhang, D.F. Yang, J.X. Du, H.L. Sun, L.W. Li, L.C. Wang, et al., A review of SOH prediction of Li-ion batteries based on data-driven algorithms, *Energies*. 16 (7) (2023) 3167.
- [32] L. Wang, L. Xie, Y. Yang, Y. Zhang, K. Wang, Cheng S.-j. distributed online voltage control with fast PV power fluctuations and imperfect communication, *IEEE Trans. Smart Grid* 14 (5) (2023) 3681–3695.
- [33] Q. Li, D. Li, K. Zhao, L. Wang, K. Wang, State of health estimation of lithium-ion battery based on improved ant lion optimization and support vector regression, *J. Energy Storage* 50 (2022) 104215.
- [34] M. Lewerenz, J. Munnix, J. Schmalstieg, S. Kabitz, M. Knips, D.U. Sauer, Systematic aging of commercial LiFePO₄\Graphite cylindrical cells including a theory explaining rise of capacity during aging, *J. Power Sources* 345 (2017) 254–263.
- [35] H.H. Goh, Z.T. Lan, D.D. Zhang, W. Dai, T.A. Kurniawan, K.C. Goh, Estimation of the state of health (SOH) of batteries using discrete curvature feature extraction, *J. Energy Storage* 50 (2022).
- [36] C.Q. She, Y. Li, C.F. Zou, T. Wik, Z.P. Wang, F.C. Sun, Offline and online blended machine learning for lithium-ion battery health state estimation, *IEEE T Transp. Electr.* 8 (2) (2022) 1604–1618.
- [37] C.L. Liu, Y. Zhang, J.R. Sun, Z.H. Cui, K. Wang, Stacked bidirectional LSTM RNN to evaluate the remaining useful life of supercapacitor, *Int. J. Energy Res.* 46 (3) (2022) 3034–3043.
- [38] Y.B. Che, Y.S. Liu, Z. Cheng, J.A. Zhang, SOC and SOH identification method of Li-ion battery based on SWPSO-DRNN, *IEEE J. Em. Sel. Top. P.* 9 (4) (2021) 4050–4061.
- [39] Z.H. Cui, L. Kang, L.W. Li, L.C. Wang, K. Wang, A combined state-of-charge estimation method for lithium-ion battery using an improved BGRU network and UKF, *Energy*. 259 (2022).
- [40] X. Yu, Y. Shang, L. Zheng, K. Wang, Application of nanogenerator in the field of acoustics, *ACS Appl. Electron. Mater.* 5 (9) (2023) 518–526.
- [41] M.Z. Alom, M. Hasan, C. Yakopcic, T.M. Taha, V.K. Asari, Improved inception-residual convolutional neural network for object recognition, *Neural Comput. & Applic.* 32 (1) (2020) 279–293.
- [42] H.L. Sun, D.F. Yang, L.C. Wang, K. Wang, A method for estimating the aging state of lithium-ion batteries based on a multi-linear integrated model, *Int. J. Energy Res.* 46 (15) (2022) 24091–24104.
- [43] M.F. Ng, J. Zhao, Q.Y. Yan, G.J. Conduit, Z.W. Seh, Predicting the state of charge and health of batteries using data-driven machine learning, *Nat. Mach. Intell.* 2 (3) (2020) 161–170.
- [44] Y. Guo, P. Yu, C. Zhu, K. Zhao, L. Wang, K. Wang, A state-of-health estimation method considering capacity recovery of lithium batteries, *Int. J. Energy Res.* 46 (15) (2022) 23730–23745.
- [45] X. Gu, K.W. See, P. Li, K. Shan, Y. Wang, L. Zhao, et al., A novel state-of-health estimation for the lithium-ion battery using a convolutional neural network and transformer model, *Energy*. 262 (2023) 125501.
- [46] W.L. Wang, D.F. Yang, Z.X. Huang, H. Hu, L.C. Wang, K. Wang, Electrodeless nanogenerator for dust recover, *Energ. Technol.* 10 (12) (2022) 2200699.
- [47] M. Li, G. Zhou, W. Cai, J. Li, M. Li, M. He, et al., Multi-scale sparse network with cross-attention mechanism for image-based butterflies fine-grained classification, *Appl. Soft Comput.* 117 (2022) 108419.
- [48] M.K. Tran, S. Panchal, V. Chauhan, N. Brahmabhatt, A. Mevawalla, R. Fraser, et al., Python-based scikit-learn machine learning models for thermal and electrical performance prediction of high-capacity lithium-ion battery, *Int. J. Energy Res.* 46 (2) (2022) 786–794.
- [49] K.A. Severson, P.M. Attia, N. Jin, N. Perkins, B. Jiang, Z. Yang, et al., Data-driven prediction of battery cycle life before capacity degradation, *Nat. Energy* 4 (5) (2019) 383–391.
- [50] W. He, N. Williard, M. Osterman, M. Pecht, Prognostics of lithium-ion batteries based on Dempster-Shafer theory and the Bayesian Monte Carlo method, *J. Power Sources* 196 (23) (2011) 10314–10321.
- [51] Y.J. Xing, E.W.M. Ma, K.L. Tsui, M. Pecht, An ensemble model for predicting the remaining useful performance of lithium-ion batteries, *Microelectron. Reliab.* 53 (6) (2013) 811–820.
- [52] Z.B. Wei, H.K. Ruan, Y. Li, J.W. Li, C.Z. Zhang, H.W. He, Multistage state of health estimation of lithium-ion battery with high tolerance to heavily partial charging, *IEEE T Power Electr.* 37 (6) (2022) 7432–7442.
- [53] Y. Guo, D. Yang, Y. Zhang, L. Wang, K. Wang, Online estimation of SOH for lithium-ion battery based on SSA-Elman neural network, *Prot. Contr. Modern Power Syst.* 7 (1) (2022) 40.
- [54] S. Bockrath, V. Lorentz, M. Pruckner, State of health estimation of lithium-ion batteries with a temporal convolutional neural network using partial load profiles, *Appl. Energy* 329 (2023) 120307.
- [55] H. Sun, D. Yang, L. Wang, K. Wang, A method for estimating the aging state of lithium-ion batteries based on a multi-linear integrated model, *Int. J. Energy Res.* 46 (15) (2022) 24091–24104.
- [56] V. Chalavadi, P. Jeripothula, R. Datla, S.B. Ch, C. KM, mSODANet: a network for multi-scale object detection in aerial images using hierarchical dilated convolutions, *Pattern Recogn.* 126 (2022) 108548.
- [57] O. Abedinia, N. Amjadi, H. Zareipour, A new feature selection technique for load and price forecast of electrical power systems, *IEEE T Power Syst.* 32 (1) (2017) 62–74.
- [58] H.K. Ruan, Z.B. Wei, W.T. Shang, X.C. Wang, H.W. He, Artificial intelligence-based health diagnostic of Lithium-ion battery leveraging transient stage of constant current and constant voltage charging, *Appl. Energy* 336 (2023).
- [59] X.S. Hu, Y.H. Che, X.K. Lin, S. Onori, Battery health prediction using fusion-based feature selection and machine learning, *IEEE T Transp. Electr.* 7 (2) (2021) 382–398.
- [60] H. Xu, L. Wu, S. Xiong, W. Li, A. Garg, L. Gao, An improved CNN-LSTM model-based state-of-health estimation approach for lithium-ion batteries, *Energy*. 276 (2023) 127585.
- [61] Y. Ma, M. Yao, H. Liu, Z. Tang, State of health estimation and remaining useful life prediction for lithium-ion batteries by improved particle swarm optimization-back propagation neural network, *J. Energy Storage* 52 (2022) 104750.
- [62] T. Bai, H. Wang, Convolutional-transformer-based multiview information perception framework for lithium-ion battery state-of-health estimation, *IEEE Trans. Instrum. Meas.* 72 (2023) 1–12.

- [63] L. Chen, S. Xie, A.M. Lopes, X. Bao, A vision transformer-based deep neural network for state of health estimation of lithium-ion batteries, *Int. J. Electr. Power Energy Syst.* 152 (2023) 109233.
- [64] K. Luo, H. Zheng, Z. Shi, A simple feature extraction method for estimating the whole life cycle state of health of lithium-ion batteries using transformer-based neural network, *J. Power Sources* 576 (2023) 233139.
- [65] M. Zhang, W. Wang, G. Xia, L. Wang, K. Wang, Self-powered electronic skin for remote human-machine synchronization, *ACS Appl. Electron. Mater.* 5 (1) (2023) 498–508.
- [66] D. Wang, Y. Yang, T. Gu, A hierarchical adaptive extended Kalman filter algorithm for lithium-ion battery state of charge estimation, *J. Energy Storage* 62 (2023) 106831.
- [67] M. Jiao, D. Wang, The Savitzky-Golay filter based bidirectional long short-term memory network for SOC estimation, *Int. J. Energy Res.* 45 (13) (2021) 19467–19480.
- [68] M. Jiao, D. Wang, Y. Yang, F. Liu, More intelligent and robust estimation of battery state-of-charge with an improved regularized extreme learning machine, *Eng. Appl. Artif. Intell.* 104 (2) (2021), 104407.